Power Grid Topology Inference Using Power Line Communications

Lutz Lampe and Mohamed O. Ahmed
Department of Electrical and Computer Engineering, The University of British Columbia, Vancouver, BC, Canada
Email: {lampe,mohameda}@ece.ubc.ca

***Abstract*— Power line communications (PLC) is one of the communication methods currently deployed and developed further to support smart grid applications. While the fact the PLC signals travel through power lines makes reliable communication more challenging than for other wired media, it also provides one distinct advantage: PLC signals can be used to learn about the grid status. In this paper, we exploit this "through the grid" property of PLC for the purpose of inferring the topology of the power grid to which a PLC network is deployed. In particular, we present a topology estimation algorithm that only requires PLC signaling between the end points of a grid, such as between meters and data concentrator in an advanced meter management system. Our methodology is alike network tomography used to infer internal properties of a communication network based on end-to-end measurements, and we refer to it as tomography-based topology inference.**

***Index Terms*— Smart grid, power line communications, topology inference, online diagnostics.**

I. Introduction

Power line communications (PLC), which reuses power lines for the purpose of data communications, has been used by electric utility companies for about a century [1], [2]. Since the late 1990's, PLC technology has experienced major innovations. While the first wave of innovation targeted broadband PLC for multimedia communications, more recently narrowband and broadband PLC for smart grid applications has been the focus of research and development, e.g. [3]–[7].

The main purpose of PLC for smart grid is to enable applications that require communications. In doing so, PLC is challenged by the fact that the power grid was not designed to support high-frequency signal propagation. Signal attenuation and reflection at discontinuities are two of the main effects experienced by PLC signals traveling through the grid. However, while the binding of the PLC signal to the power lines makes communication challenging, it also enables another use of PLC, especially in the context of smart grid. That is, observing the PLC signal after being sent through the power grid allows us to learn about the grid, i.e., to perform grid diagnostics. This property is unique to PLC, being the only "through the grid" [5] communication technology.

The use of high-frequency signals traveling through power lines for diagnostics is not a new idea. For example, fault localization based on measuring traveling waves emitted from faults at different ends of power lines or by sending a stimulating signal which propagates along the line and reflects at the fault location are described in [8, Ch. 7] and [9], [10], respectively. Another example is the prediction of line failures based on the strength of the PLC signals in a smart metering system, which has been suggested in [11].

In this paper, we consider a different diagnostics application of PLC, which is grid topology inference, also referred to as topology estimation [12]. We assume that a PLC network consisting of a set of PLC modems is in place, for example for the purpose of supporting an advanced meter management (AMM) infrastructure. These modems communicate with each other, and the time of flight of the communication signal enables a distance estimation for the communication link, i.e., ranging. Then, based on the ranging between pairs of nodes in the grid, we use a network tomography approach to infer the underlying grid structure. Tomography is a methodology that tries to reconstruct the internal properties of an object based on observations from sensors surrounding it. It has been used in communication networks for inferring e.g. link performance, routing topologies, etc. based on end-to-end measurements, cf. e.g. [13]. By formulating power-grid-topology inference using distance measurements as a tree estimation problem, it becomes analogous to those considered in the communication network applications. Hence, we refer to the proposed method as tomography-based topology inference.

Our work is related to topology estimation presented in [12], [14]. These works use distance and topology estimation to optimize the use of distributed energy sources in smart micro grids. Different from our work, it is assumed that all branch points in the grid are equipped with PLC modems. Such an assumption would not hold true for, for example, a low-voltage distribution grid with PLC modems deployed at electricity meters and communicating with modems at one (or multiple) transformer stations connecting the low-voltage domain to the rest of the grid. Our approach is also mostly targeting topology inference in low-voltage distribution grids. One application is to enable electric utility companies to map these parts of the grid. Not having such a mapping of the low-voltage grid is a real problem for utilities and prevents them from, for example, automatic identification of faulty cables [15]. Another application is the support of PLC routing. The use of location information for PLC routing was presented in [16]. The proposed topology inference method would provide the required location information, similar to location services in geographic routing for wireless communication networks. Another application area is the support of the smart grid operation through online monitoring and diagnostics. This includes optimization of smart micro grids as considered in

This work was supported by the Natural Sciences and Engineering Research Council (NSERC) of Canada.

[12], [14], and more generally online monitoring of grid elements including loads and lines, similar to the application examples considered in [9]–[11]. Furthermore, smart fault location systems using intelligent electronic devices as discussed in [17] would also benefit from updated grid-topology information.

To present the new topology inference method, in Section II we introduce a graph representation of the power grid as well as the principles of PLC signal propagation modeling applied for obtaining numerical results. Then, in Section III, we introduce the new tomography-based topology estimation method. Numerical results demonstrating the performance of our method are presented and discussed in Section IV. Final remarks in Section V conclude this paper.

II. Graph Representation of and Signal Propagation Through the Grid

In this section, we first introduce the abstract description of (a part of) the grid consisting of grid elements connected through power lines. Then, we briefly review the applied model for PLC signal propagation.

A. Graph Representation

The electricity grid we consider consists of electrical "devices", such as for example power generators, transformers, energy storage units, or energy loads, which are connected through power lines (overhead or underground). The devices of interest are equipped with a PLC modem and the set of modems forms a PLC network. The PLC network is likely put in place to perform a smart-grid communication task, such as automatic meter reading, supporting supervisory control and data acquisition systems, transmitting pricing information, etc. In this case, their use for topology estimation does not entail any additional installation or equipment costs.

We can describe the electricity grid under investigation as a bi-partite graph consisting of vertices (or nodes), representing the devices, and edges, representing the power lines. Figure 1 shows such a graph representing a smart micro grid with 30 nodes from [12]. Another graph corresponding to an AMM infrastructure considered in [18] is shown in Figure 2. The authors of [12] assume that all nodes are PLC enabled. However, for the AMM system in Figure 2, only the leaf nodes (filled circles in Figure 2), representing the meters, are PLC nodes, whereas the internal nodes (circles in Figure 2), representing branch points or taps, are not equipped with PLC modems. What both topologies have in common is a tree structure. In fact, tree topologies are quite common for the distribution domain of the grid, as well as for indoor scenarios, cf. also e.g. [2, Figures 2.16, 2.47], [19]–[21]. We will assume a tree structure in the following.

B. PLC Signal Propagation

The propagation of PLC signals through power lines can be described using two approaches. The first is a phenomenological approach. In this case, parameters of a model that captures the multipath propagation and distance- and frequency-dependant attenuation are adjusted based on measurements of

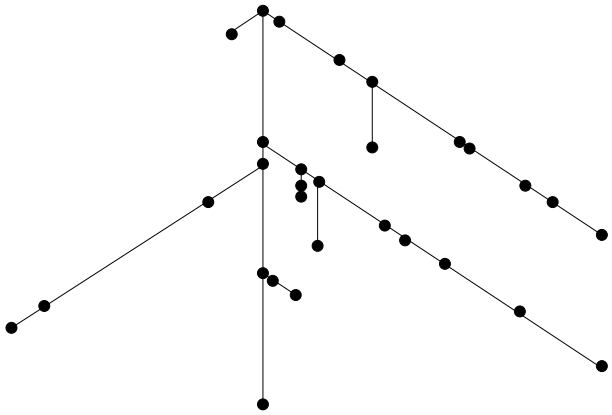

Fig. 1. Sample graph for a grid topology representing a smart micro grid. From Figure 1 in [12].

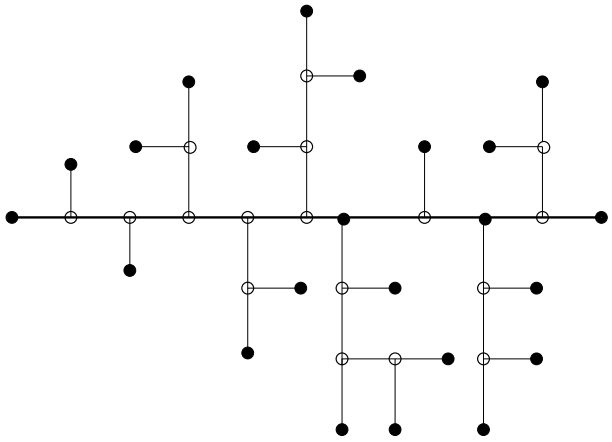

Fig. 2. Sample graph for a grid topology representing low-voltage distribution grid. From Figure 8 in [18]. Internal nodes are represented by circles, while leaf nodes (at which PLC modems are deployed) are represented by filled circles.

channel transfer functions. Such a model has been adopted in [12]. The second approach is deterministic. It is based on the knowledge of the relevant electromagnetic properties of the grid elements, i.e., lines and loads, as well as the line lengths, and uses transmission line theory to determine the channel transfer functions. The latter is more suitable for the situation at hand, as it enables us to simultaneously compute the transfer functions of all PLC links in a network. It is important to note that these transfer functions are interdependent and that this interdependence is neglected in a phenomenological approach, which inherently considers individual links in isolation. Secondly, the effect of loads on the signal propagation is taken into consideration, which again is neglected in the phenomenological approach. For these reasons, we adopt this approach for the numerical results presented in Section IV. For more details we refer to [2, Chapter 2].

III. Topology Inference

The main objective of topology estimation is to recover the graph structure and thus the grid topology as shown in Figures 1 and 2. This means that both the connection of nodes as well as the length of edges are estimated. In this section, we introduce our new tomography-based method, which, different from [12], allows us to infer topologies where not every node

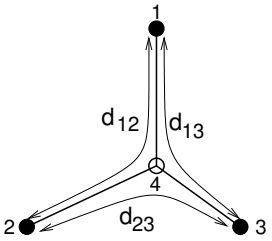

Fig. 3. Illustration of tomography-based approach for a 4-node topology.

is equipped with a PLC modem. Our method relies on ranging between PLC nodes. We refer to [12] for the details of this ranging, and further extensions are discussed in the journal version of this work [22].

A. Tomography-based Inference

As mentioned above, the neighborhood-based approach from [12] cannot be applied to topologies and PLC networks such as in Figure 2, where only leaf nodes are equipped with PLC modems. A typical example would be an AMM system, where PLC transceivers are installed at electricity meters. For this scenario, we propose a new topology inference algorithm.

Our approach relies on ranging using PLC signals. Since PLC modems are only deployed at leaf nodes, we cannot assume that distances between all nodes are estimated, but only between leaf nodes. The following example illustrates how these end-to-end measurements can be used to infer the topology. Consider a network with four nodes as shown in Figure 3. Enumerating the nodes by $i = 1, 2, 3, 4$ and denoting the (node i)-to-(node j) distance by d_{ij}, then we can identify the internal node 4 using end-to-end ranging measurements from

$$\begin{aligned} d_{12} &= d_{14} + d_{24} \\ d_{13} &= d_{14} + d_{34} \\ d_{23} &= d_{24} + d_{34} \end{aligned} \tag{1}$$

For example, the solution for d_{14} is

$$d_{14} = \frac{d_{12} + d_{13} - d_{23}}{2} \, . \tag{2}$$

The end-to-end measurements completely determine the tree topology. Note that the different cases of line topologies are included via the solutions $d_{14} = 0$ or $d_{24} = 0$ or $d_{34} = 0$.

The above approach can be easily extended to the case of $N > 3$ leaf nodes as follows. First, one node is declared a root node. Let us assume that node 1 is this node. Then, pairs of leaf nodes with a common parent node are determined. To this end, the distances d_{1x} between hypothetical parent nodes x and the root node are computed as in (2) for all possible pairs of leaf nodes. The node x^* with the longest distance must indeed be a parent node and thus, an internal node connecting two leaf nodes has been identified. This node now replaces the two leaf nodes, and the procedure is continued until no leaf node is left.

Interestingly, the presented algorithmic method for topology inference has long been used for inferring phylogenetic trees in evolutionary biology. In this application case, distance measures suitable to characterize similarities between extant species are applied as end-to-end "measurements", and then the described inference is applied to obtain evolutionary relationships. More specifically, the inference algorithm is known as the neighbor-joining algorithm (NJA) developed in [23]. More recently, the NJA has been applied to network tomography in [24] by Ni and Tatikonda. They also present the rooted version of the NJA, the rooted NJA (RNJA), which is based on (2). A pseudo-code for the key steps of the RNJA as described above and following [24] is shown as Algorithm 1 below.

Input: Distance measurements between all leaf nodes, $i = 1, \ldots, K$.
Output: Topology and distances between all grid nodes
// Initialization
Root node $s = 1$, set of leaf nodes of inspected tree $\mathcal{D} = \{2, \ldots, K\}$, Enumerator for new nodes $f = K$
// Go through all leaf nodes
while $|\mathcal{D}| > 1$ **do**
  // Compute distance between root node and nearest common parent node of i and j (see (2))
  for $i, j \in \mathcal{D}$ **do**
    $q_{ij} = \frac{1}{2}(d_{si} + d_{sj} - d_{ij})$
  end for
  // Nodes that maximize distance are neighbors
  $(i^*, j^*) = \underset{(i,j)}{\operatorname{argmax}} \, q_{ij}$
  // Add a new node f, the parent of i^* and j^*
  $f \leftarrow f + 1$
  // Remove i^* and j^* from the list of leaf nodes
  $\mathcal{D} \leftarrow \mathcal{D} \setminus \{i^*, j^*\}$
  // Compute distances from s, i^*, j^* to new node f
  $d_{sf} = q_{i^*j^*}$, $d_{fi^*} = d_{si^*} - q_{i^*j^*}$, $d_{fj^*} = d_{sj^*} - q_{i^*j^*}$
  // Compute distance from leaf nodes to new node f
  for $k \in \mathcal{D}$ **do**
    $d_{kf} = \frac{1}{2}(d_{ki^*} - d_{fi^*}) + \frac{1}{2}(d_{kj^*} - d_{fj^*})$,
    $q_{kf} = \frac{1}{2}(q_{ki^*} + q_{fj^*})$
  end for
  // New node becomes leaf node of inspected tree
  $\mathcal{D} \leftarrow \mathcal{D} \cup \{f\}$
end while

Algorithm 1: Rooted neighbor-joining algorithm (following [24]).

The RNJA and thus the tomography-based topology estimation approach are remarkably robust to distance estimation errors. As long as the ranging error for any distance estimate is below half the minimal edge length of the topology graph, Algorithm 1 returns the correct topology, i.e., the correct tree structure of the topology graph. Of course, ranging errors affect the accuracy of the estimated edge lengths in the graph.

We note that Algorithm 1 is formulated for binary trees, i.e., a parent node splits into two children nodes. This encompasses a large number of low-voltage grid topologies for which PLC-based topology inference is applicable, including the topologies shown in Figures 1 and 2. However, the RNJA and thus our method can be extended to general trees with only a slight modifications as shown in [24].

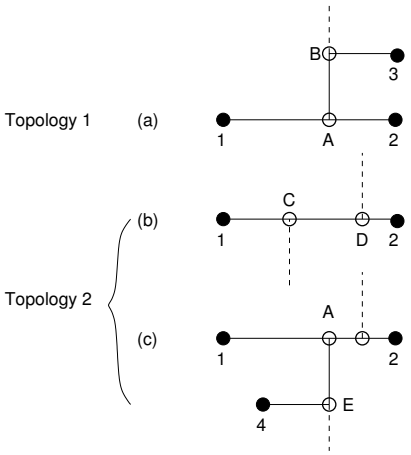

Fig. 4. Illustration of scenarios when merging two partial topologies (Topologies 1 and 2).

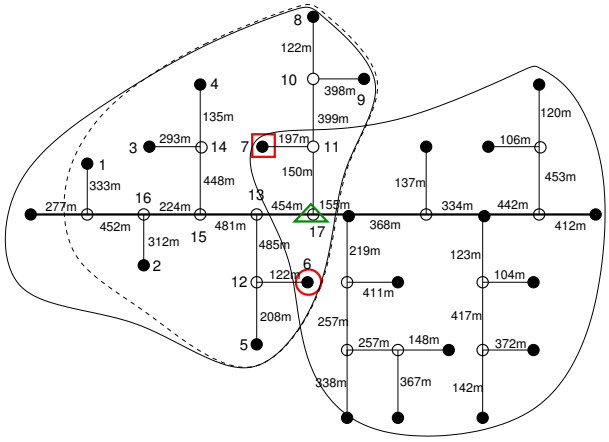

Fig. 5. Grid topology from [18] used for performance evaluation. Nodes equipped with PLC modems are represented by filled circles. Branch points are represented by circles. Edge labels are distances. Dashed-lined and solid-line circled areas are used for ranging accuracy and topology estimation tests.

B. Localized Version

The presented topology estimation algorithm requires ranging measurements. That is, a direct link (i.e., without a relay) between modems within the PLC network must exist. Considering practical grid topologies to which PLC is applied, the requirement of connectivity without relays may be too strong. For example, distances between end nodes in the network in Figure 2 exceed 3 km (see [18]), which is typically too long for a (reliable) direct link, especially for a distribution grid with many branches and when using broadband PLC. Therefore, we consider a localized version of the topology estimation algorithm. Here, localized means that ranging is done among subsets of network nodes which are within the communication range of each other. The full topology inference is still done centrally. However, this is not a strong restriction, as ranging results can be communicated as any other message (e.g., meter data) through the PLC network possibly through multiple hops.

Let us consider two partial topologies, obtained from ranging measurements among subsets of nodes applied to Algorithm 1, which have two nodes in common. Figure 4(a) shows these two nodes, labelled 1 and 2, in the first topology, and along the path from node 1 to 2 a branch point, i.e., an internal node A exists. Figures 4(b) and (c) illustrate possible situations for nodes 1 and 2 in the second topology. In the first case, in Figure 4(b), the two topologies do not have internal nodes in common, i.e., nodes C and D are at different locations than node A, and thus they can directly be merged. In the second case, in Figure 4(c), node A is an internal node in both partial topologies. If the distance A-to-E is smaller than A-to-B, then node E can be located on the link A-to-B and vice versa. Now Algorithm 1 needs be run on the distance measurements between nodes 1 or 2 and 3, and 4 to determine the location of the parent node for 3 and 4. If the parent node is B or E, then this process needs to be continued. It is therefore advisable to choose partial topologies (based on the set of ranging measurements) such that they have no internal nodes in common. This can always be done for binary tree graphs.

In a practical scenario, the two cases shown in Figures 4(b) and (c) may be difficult to distinguish, since ranging inaccuracies will lead to estimation errors in the edge lengths of the reconstructed graph. Hence, if nodes A and C or D are relatively close, we suggest to always run Algorithm 1 on an overlapping subset of nodes from the two partial topologies to determine whether these are identical or distinct internal nodes.

IV. Performance Evaluation

In this section, we evaluate the performance of the proposed tomography-based topology inference. We consider the grid topology from Figure 2, which is shown again in Figure 5 with edges labeled with the branch lengths in meter (disregard the labeling of nodes, special markers, and grouping of nodes for the moment). We note that this topology represents a low-voltage distribution grid served by a transformer (the left-most node) [18]. The PLC nodes are located at the transformer and at the loads, which mimics an AMM scenario with communication between meters at loads and a data concentrator at the transformer. We apply the deterministic channel modeling approach described in Section II-B to compute the channel transfer functions between PLC nodes. We assume that 4-conductor cables of type NAYY150SE are applied (see [2, Section 2.3.3.1] for details). The load impedance values are as specified in [18, Figure 8].

We first consider the accuracy of ranging using PLC transmission, which is underlying to the tomography approach. For concreteness, we apply two-way ranging based on energy-detection time-of-arrival estimation as described in [14]. The PLC modems transmit with a power spectral density of -55 dBm/Hz in the frequency band of 2 MHz to 28 MHz as typical for broadband PLC, and the receiver-side noise power spectral density (PSD) is -110 dBm/Hz. Sampling with symbol rate $T_\mathrm{s} = 1/26$ μs, integration over one symbol interval, and a relative threshold of $\lambda = 0.8$ are applied for the energy detector, respectively, see [14, Eq. (17)]. The two-way time-of-flight is translated into distance estimates using the phase velocity value of $v_\mathrm{p} = 1.5 \cdot 10^8$ m/s.

Table I presents the achieved ranging accuracies in terms of the empirical mean value and standard deviation for the

TABLE I

MEAN AND STANDARD DEVIATION OF THE ABSOLUTE RANGING ERROR FOR PATHS OF DIFFERENT LENGTHS BETWEEN THE NINE NODES IN THE PART OF THE TOPOLOGY IN FIGURE 5 ENCIRCLED BY THE DASHED LINE.

Distance in meter								
Node	2	3	4	5	6	7	8	9
1	1106	1750	1592	2183	2097	2291	2615	2891
2		1286	1128	1719	1633	1827	2151	2427
3			428	1915	1829	2023	2347	2623
4				1757	1671	1865	2189	2465
5					330	1494	1818	2094
6						1408	1732	2008
7							718	994
8								520
Mean value of absolute ranging error in meter								
Node	2	3	4	5	6	7	8	9
1	6.7	2.7	5.0	2.5	2.0	3.6	6.6	25.6
2		5.4	2.1	4.7	4.3	1.8	2.7	3.4
3			4.4	3.1	4.2	1.7	3.5	4.4
4				1.5	1.9	3.0	3.2	4.5
5					4.4	5.0	3.7	2.8
6						4.5	3.4	3.1
7							2.7	3.4
8								4.6
Standard deviation of absolute ranging error in meter								
Node	2	3	4	5	6	7	8	9
1	0.0	0.0	0.2	1.2	1.4	2.0	5.0	169.0
2		0.0	0.8	0.8	0.1	2.3	2.5	3.3
3			0.0	1.9	0.7	2.2	3.1	4.0
4				0.6	2.2	0.0	2.3	2.9
5					0.0	0.0	0.4	1.7
6						0.0	0.0	1.1
7							0.0	0.0
8								0.0

absolute ranging error obtained for different links in 1000 experiments. The subset of nine nodes which are encircled by the dashed line in Figure 5 are considered. For clarity, these nodes are enumerated in Figure 5 and Table I, and the table also includes the distances between every pair of nodes. We observe that accuracies within a few meters are generally achieved. In fact, the very low standard deviation for many of the links, mostly with lengths of less than 2 km, indicates that the resolution of the PLC signal, which corresponds to $T_{\mathrm{s}} v_{\mathrm{p}} = 5.8$ m, limits accuracy. Fine tuning of the sampling rate T_{s}, threshold λ, and integration interval for the energy detector could improve this accuracy. We further note a fairly large mean error and standard deviation for the longest link of 2891 m, which shows the limitations of PLC-based ranging due to signal attenuation and thus low signal-to-noise ratio.

The ranging measurements discussed above are now input to the tomography-based topology inference algorithm presented in Section III. In particular, one set of ranging measurements between the nine nodes is used for topology inference. Figure 6 shows the reconstructed topology corresponding to the part of the entire topology in Figure 5 encircled by the dashed line. Comparing the tree in Figure 6 with the partial topology in Figure 5, we observe that the topology is correctly reconstructed. In particular, the internal nodes (nodes 10 to 16) are found correctly, and the lengths of the branches are recovered fairly accurately. The maximal error is 8 m, which occurs for the link to node 9 and which is due to the fact that

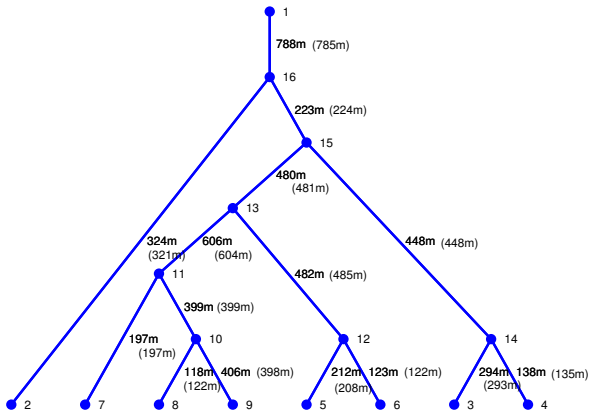

Fig. 6. Example of a reconstructed partial topology for the nine nodes encircled by the dashed line in Figure 5 using the tomography-based method. The numbers at the edges are the distances as inferred by the algorithm, and the actual distances are shown in parentheses. Internal nodes (branch points in Figure 5) 10 to 16 are created by the algorithm.

node 9 is part of the longest link and thus the largest ranging error, as shown in Table I. Hence, even higher accuracy in terms of estimated branch lengths can be achieved if a smaller subset of nodes, say nodes 1 to 8, is only considered for topology reconstruction.

We now move on to reconstruct the entire topology shown in Figure 5. Due to the large distances between nodes in this topology, we divide it into two overlapping parts, as indicated by the solid-line encircled areas in Figure 5. The overlap would not be chosen a-priori (as the topology layout may be mostly or completely unknown), but after the first partial topology reconstruction has been executed. Figures 7 and 8 show the two estimated topologies. A comparison between these two trees and Figure 5 confirms that the partial topologies are faithfully reconstructed. Furthermore, as can be seen from the estimated and true (in parentheses) branch lengths shown in Figures 7 and 8, the reconstruction is fairly accurate in terms of distances. If desired, accuracy can further be improved by dividing the topology into more partial topologies.

For combining the two reconstructed partial topologies, nodes 6 and 7 from the partial topology in Figure 7 (see Figure 5 for node numbering) have been included in the estimation of the second partial topology in Figure 8. The nodes are identified by the larger markers in the figures. They would be chosen as they are within the communication range of all other nodes of the respective partial topologies. Considering the paths between these two nodes in the trees in Figures 7 and 8, we observe that we have a case as illustrated in Figures 4(a) and (b). That is, the branch points on these paths do not coincide, even when taking into account estimation errors for the branch lengths in the reconstruction. Hence, the combination of the two partial topologies is obtained by including the subtree with the root-node identified with the triangle marker in Figure 8, which is the internal node 17 in Figure 5, at the edge also identified with a triangle marker in Figure 7. This completes the topology inference for this example.

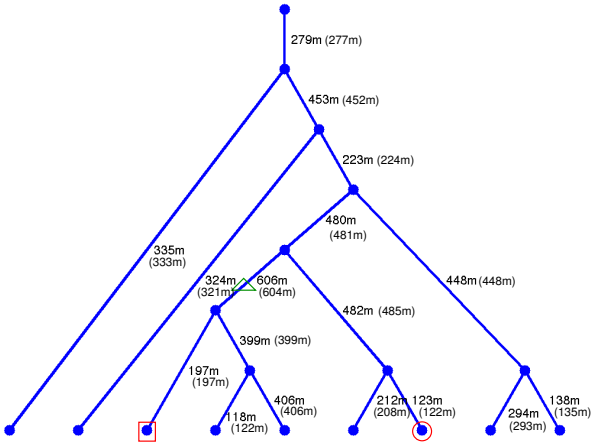

Fig. 7. Reconstructed partial topology for the nodes encircled by the solid line on the *left* side of Figure 5 using the tomography-based method. The numbers at the edges are the distances as inferred by the algorithm, and the actual distances are shown in parentheses. The red and green markers identify the nodes 5, 6, and 17 from Figure 5.

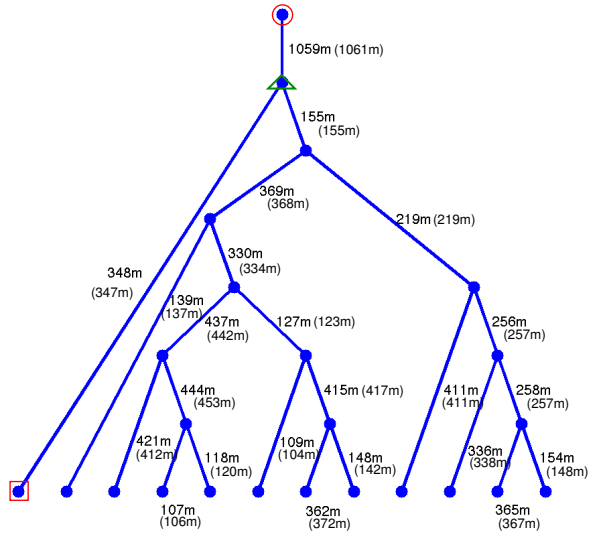

Fig. 8. Reconstructed partial topology for the nodes encircled by the solid line on the *right* side of Figure 5 using the tomography-based method. The numbers at the edges are the distances as inferred by the algorithm, and the actual distances are shown in parentheses. The red and green markers identify the nodes 5, 6, and 17 from Figure 5.

V. Conclusions

In this paper, we have introduced a grid-topology inference method that is based on distance estimation using PLC signals followed by a topology reconstruction algorithm, which has been borrowed from the network tomography community. Since our method relies on end-to-end measurements to infer the entire topology including its internal structure, we refer to it as tomography-based inference. Our method can be used for a number of applications in smart grids, including optimization of energy generation and consumption [14], fault identification [15], PLC routing [16], online monitoring and smart fault localization [9]–[11], [17]. Our numerical results for a typical low-voltage distribution grid example have clearly demonstrated the capabilities of tomography-based topology estimation. Further improvements in accuracy can be achieved through more accurate ranging methods. In the journal version of this work [22] we elaborate further on this and also introduce a new parametric ranging algorithm.

References

[1] H. C. Ferreira, H. M. Grov, O. Hooijen, and A. J. Han Vinck, *Power Line Communication*. John Wiley & Sons, 2001. [Online]. Available: http://dx.doi.org/10.1002/047134608X.W2004

[2] H. Ferreira, L. Lampe, J. Newbury, and T. Swart (Editors), *Power Line Communications: Theory and Applications for Narrowband and Broadband Commun. over Power Lines*. John Wiley & Sons, 2010.

[3] H. Latchman and L. Younge (Guest Editors), "Power line local area networking," *IEEE Commun. Mag.*, vol. 41, no. 4, pp. 32–33, 2003.

[4] S. Galli, A. Scaglione, and K. Dostert (Guest Editors), "Broadband is power: Internet access through the power line network," *IEEE Commun. Mag.*, vol. 41, no. 5, pp. 82–83, 2003.

[5] S. Galli, A. Scaglione, and Z. Wang, "For the grid and through the grid: The role of power line communications in the smart grid," *Proc. IEEE*, vol. 99, no. 6, pp. 998–2017, 2011.

[6] S. Bavarian and L. Lampe, "Physical communications and access techniques for smart grid," in *Smart Grid Commun. and Netw.*, E. Hossain, Z. Han, and H. Poor, Eds. Cambridge University Press, 2012.

[7] L. Lampe, A. Tonello, and D. Shaver, "Power line communications for automation networks and smart grid [guest editorial]," *IEEE Commun. Mag.*, vol. 49, no. 12, pp. 26 –27, Dec. 2011.

[8] IEEE Std C37.114^{TM}-2004, "IEEE Guide for Determining Fault Location on AC Transmission and Distribution Lines," Jun. 2005.

[9] V. Taylor and M. Faulkner, "Line monitoring and fault location using spread spectrum on power line carrier," *IEE Proceedings-Generation, Transmission and Distribution*, vol. 143, no. 5, pp. 427 –434, Sep. 1996.

[10] A. N. Milioudis, G. T. Andreou, and D. P. Labridis, "Enhanced protection scheme for smart grids using power line communications techniques — Part II: Location of high impedance fault position," *IEEE Trans. Smart Grid*, vol. 3, no. 4, pp. 1631–1640, 2012.

[11] R. Rao, S. Akella, and G. Guley, "Power line carrier (PLC) signal analysis of smart meters for outlier detection," in *IEEE International Conference on Smart Grid Communications (SmartGridComm)*, Oct. 2011, pp. 291 –296.

[12] T. Erseghe, S. Tomasin, and A. Vigato, "Topology estimation for smart micro grids via powerline communications," *IEEE Trans. Signal Processing*, 2013, available on IEEEXplore.

[13] R. Castro, M. Coates, G. Liang, R. Nowak, and B. Yu, "Network tomography: Recent developments," *Statistical Science*, vol. 19, no. 3, pp. 499–517, 2004.

[14] T. Erseghe, F. Lorenzon, S. Tomasin, A. Costabeber, and P. Tenti, "Distance measurement over PLC for dynamic grid mapping of smart micro grids," in *IEEE Smart Grid Communications (SmartGridComm)*, Brussels, Belgium, Oct. 2011, pp. 487–492.

[15] A. Goedhart, "Personal communications."

[16] M. Biagi and L. Lampe, "Location assisted routing techniques for power line communication in smart grids," in *IEEE International Conference on Smart Grid Communications (SmartGridComm)*, Oct. 2010.

[17] M. Kezunovic, "Smart fault location for smart grids," *IEEE Trans. Smart Grid*, vol. 2, no. 1, pp. 11 –22, Mar. 2011.

[18] G. Prasanna, A. Lakshmi, S. Sumanth, V. Simba, J. Bapat, and G. Koomullil, "Data communication over the smart grid," in *Intl. Symp. Power Line Commun. (ISPLC)*, Mar./Apr. 2009, pp. 273–278.

[19] G. Bumiller, L. Lampe, and H. Hrasnica, "Power line communication networks for large-scale control and automation systems," *IEEE Commun. Mag.*, vol. 48, no. 4, pp. 106 –113, Apr. 2010.

[20] S. Goldfisher and S. Tanabe, "IEEE 1901 access system: An overview of its uniqueness and motivation," *IEEE Commun. Mag.*, vol. 48, no. 10, pp. 150–157, Oct. 2010.

[21] L. Dho and R. Lehnert, "Dynamic resource allocation protocol for large PLC networks," in *Intl. Symp. Power Line Commun. (ISPLC)*, Beijing, China, Mar. 2012, pp. 41–46.

[22] M. Ahmed and L. Lampe, "Power line communications for power grid tomography," *submitted for publication*, 2013. [Online]. Available: http://www.ece.ubc.ca/~lampe/Preprints/PLC_Tomography.pdf

[23] N. Saitou and M. Nei, "The neighbor joining method: a new method for reconstructing phylogenetic trees," *Molecular Biology and Evolution*, vol. 4, no. 4, pp. 406–425, 1987.

[24] J. Ni and S. Tatikonda, "Network tomography based on additive metrics," *IEEE Trans. Inform. Theory*, vol. 57, no. 12, pp. 7798–7809, Dec. 2011.